

# We are IntechOpen, the world's leading publisher of Open Access books Built by scientists, for scientists

6,900

Open access books available

186,000

International authors and editors

200M

Downloads

Our authors are among the

154

Countries delivered to

TOP 1%

most cited scientists

12.2%

Contributors from top 500 universities



WEB OF SCIENCE™

Selection of our books indexed in the Book Citation Index  
in Web of Science™ Core Collection (BKCI)

Interested in publishing with us?  
Contact [book.department@intechopen.com](mailto:book.department@intechopen.com)

Numbers displayed above are based on latest data collected.  
For more information visit [www.intechopen.com](http://www.intechopen.com)



# Application of remote sensing to the estimation of sea ice thickness distribution

Takenobu Toyota  
Hokkaido University  
Japan

## 1. Introduction

Sea ice covers about one tenth of the world ocean surface and plays an important role in the global climate system through its interaction with the atmosphere and ocean. Although its thickness is only several meters at most, it forms an effective thermal insulation sheet due to its high albedo and low thermal conductivity, leading to a significant reduction in the heat flux from the ocean to the atmosphere, especially in winter. Moreover, when sea ice forms, it expels brine into water to produce high density water underneath the ice, leading to the deep vertical convection. This plays a major role in the three dimensional ocean thermohaline circulation of the ocean on a global scale. Another notable feature is its large variability in areal extent on seasonal to annual time scales e.g. in the Southern Hemisphere (Figure 1). Even on a daily time scale, it varies significantly due to the combined effects of wind and ocean swell. In turn this variability also has an impact on both climate and daily weather conditions through the above processes. In addition, the mobility of sea ice leads to the interaction between ice floes and ridging/rafting of the ice (dynamical pile-up), which makes its properties more complex in comparison with other surface types in the cryosphere, such as snow cover or frozen soil.

In these processes, thickness distribution is one of the most important parameters of sea ice. This is firstly because the outgoing heat flux from ocean to atmosphere is highly dependent on the ice thickness distribution, especially in winter when the areal fraction of ice with a thickness of less than 0.4 m essentially controls the net heat input to the atmosphere (Maykut, 1978). This implies that the areal fraction of thin ice controls the rates of thermodynamic ice growth amount and the associated production of the high density water beneath. Therefore, the ice thickness distribution can make a significant difference to both the surface heat budget and deep ocean convection for a given concentration of sea ice. In this context, it is worth mentioning that snow cover on ice also works as a more effective insulator due to its low thermal conductivity. Secondly, and in terms of sea ice dynamics, the thickness distribution determines ice strength, and thus controls ridging/rafting processes and vice versa (Thorndike et al., 1975). These “pile-up” processes are essential to the ice thickening, particularly in the seasonal sea ice zone (SSIZ) where the ice is relatively thin and mobile. From the crystallographic analyses it has been shown that a layered structure due to ice pile-up is prominent in the SSIZ (e.g. Gow et al., 1982; Lange and Eicken,

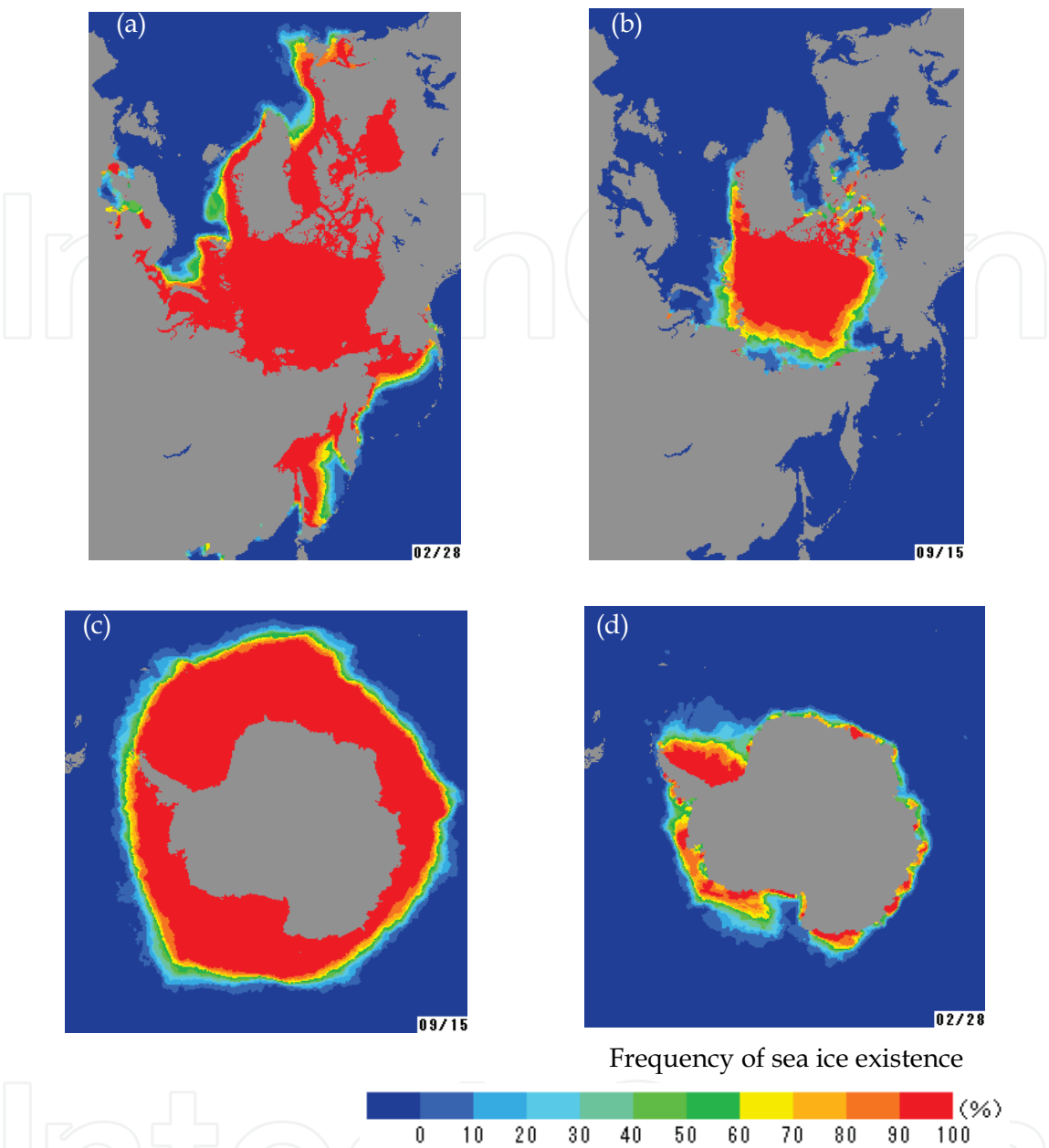


Fig. 1. Mean geographical distribution of sea ice extent (1979-2000) for the northern hemisphere at (a) maximum extent (Feb. 28) and (b) minimum extent (Sep. 15) the southern hemisphere at (c) maximum extent (Sep. 15) and (d) minimum extent (Feb. 28). (Japan Meteorological Agency, 2005)

1991) and that the mean layer thickness is only about 12 cm both for Antarctic ice (Worby et al., 1996) and that in Arctic peripheral seas e.g. the Sea of Okhotsk (Toyota et al., 2007). Therefore, the observed thickness distribution can provide some important insights into the role of such dynamical thickening processes. Thirdly, the long-term trend and the short-term change in the sea ice thickness distribution is a sensitive indicator of climate change, as observed for Arctic perennial ice (e.g. Nghiem et al., 2007). Therefore, the accurate and

consistent estimation of sea ice thickness distribution is one of the most important issues that many researchers in this field have paid attention to for a long time.

Unfortunately, sea ice thickness is also one of the most difficult parameters to measure. It was only two decades ago that the mean hemispheric distribution of ice thickness was first mapped for the Arctic Ocean (Bourke and Garrette, 1987; Figure 2a), and only recently for the Antarctic Seas (Worby et al., 2008; Figure 2b). The most direct and accurate measurement technique is in-situ drilling with an ice auger. In the Arctic, it is said that Nansen first conducted systematic ice thickness measurement with this method during the drift of "Fram" (1893-96) (Wadhams, 2000). In the Antarctic, it was by drilling that the standard measurement protocol was initiated in the late 1970's (Ackley et al., 1979). In addition to being labour-intensive, this technique suffers a problem of representativity. Rothrock (1986) pointed out from a statistical perspective that as many as 560 drilling sites would be required if we need to know the mean thickness at a point with an accuracy of 0.1 m for the Arctic ice. Thus, nowadays this method is used mainly for calibration of other tools. To obtain thickness distribution at a large scale, remote sensing is a requisite tool. Since 1958, when submarine sonar was applied for this purpose in the Arctic Ocean, enormous efforts have been made to estimate it using remote sensing. Unfortunately, submarine sonar coverage of Antarctic ice is not possible.

In this chapter several methods will be introduced to give a brief history of ice thickness measurement, focusing on how remote sensing techniques have been applied and how they have contributed to the improved understanding of sea ice thickness. Finally, the current situation will be summarized and some suggestions will be made about a future work that needs to be done.

## 2. Measurement techniques

In this section the remote sensing tools that have been used to measure ice thickness to date will be introduced. There are generally two strategies: 1) direct measurement of ice draft or a full depth of ice using an upward-looking sonar or other tools; and 2) relating the observed surface properties with ice thickness using satellite sensors. Here, they will be described in near-chronological order.

### 2.1 Submarine sonar profiling

This method provides the under-ice profile relative to sea level using an upward beamed sonar on a submarine. By this technique, profiles of ice draft can be obtained along the track of the submarine by recording the distance to the underside of the ice pack and subtracting this from the depth of the sonar, using intervening regions of open water as a reference level. The overall accuracy is about 0.3 m (0.09 m for smooth ice), and the horizontal resolution is 1.3 to 1.5 m with a surface beam diameter of 3.2 m (Wadhams and Horne, 1980). These data are not a complete measurement of ice thickness, as ice draft corresponds to 80 to 95 % of ice thickness, but nonetheless this data set provides the approximate thickness distribution and detailed topography of under-ice with reasonable accuracy, assuming invariability in snow cover thickness and density.

This device was first used during the voyage of the "Nautilus" in early August 1958 which crossed the Arctic Basin, and much of our knowledge about the synoptic ice thickness

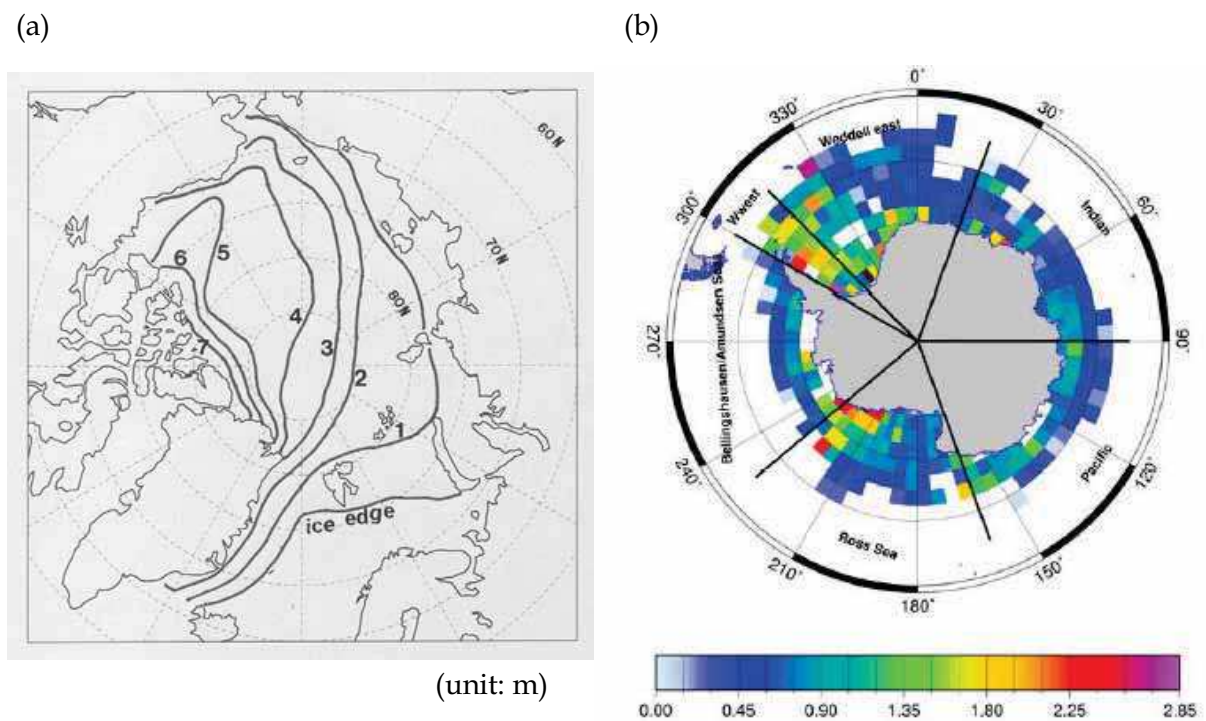


Fig. 2. Climatology of ice thickness distribution for (a) the northern hemisphere (reproduced based on Bourke & Garrett (1987)) (b) the southern hemisphere (cited from Worby et al. (2008)). The average periods are 1960-82 for the Arctic and 1981-2005 for the Antarctic. The data are based on submarine sonar observations for the Arctic and on ship-based repeated visual observations for the Antarctic.

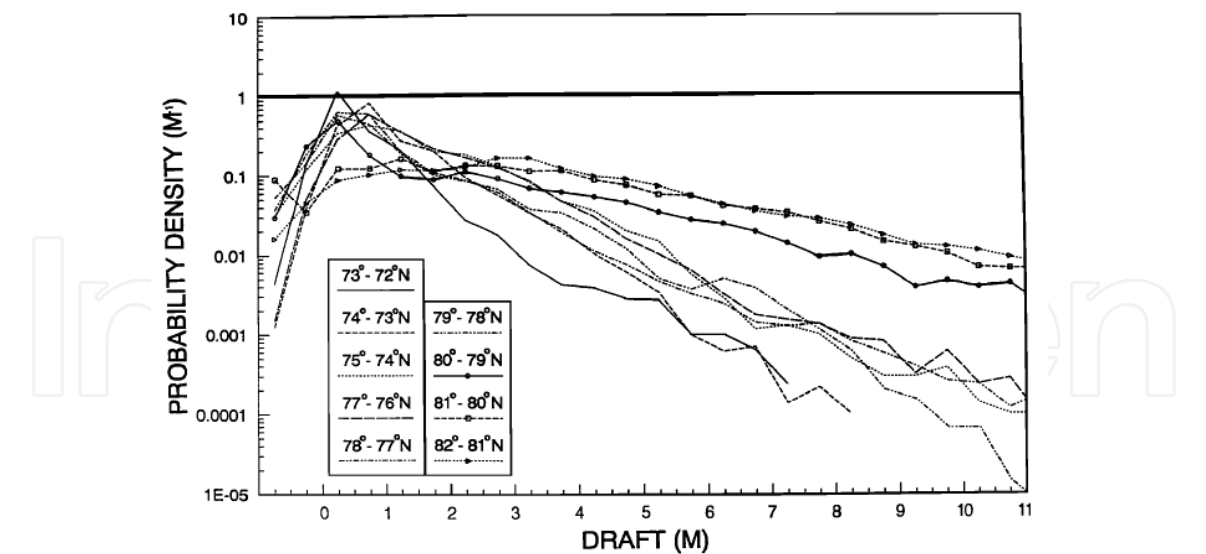


Fig. 3. Probability density of ice thickness in the Greenland Sea. Note that the clear negative exponential tail at the thick end can be seen for all the cases. (cited from Wadhams (1992)).



distribution in the Arctic Ocean is based on the results obtained with this device on subsequent cruises (McLaren, 1989). With the results obtained, the regional statistics of ice thickness distribution and ridge keel profiles were investigated in detail e.g. for the Beaufort Sea (Wadhams and Horne, 1980), in the Fram Strait region (Wadhams, 1983, 1992), and in Davis Strait (Wadhams et al., 1985). One of the most significant findings is that in most cases the thickness distribution follows a negative exponential function, irrespective of regional location (Figure 3). Although the mechanism to explain this feature has not been clarified yet, this feature may provide considerable insight into the ridging process and is therefore a problem worth investigating given that ridging is a key determinant of the thickness distribution. McLaren (1989) examined the general features for the ice over the Arctic Basin from the data sets obtained along the two identical cruises tracks in 1958 and 1970. Bourke and Garrett (1987) then compiled the data obtained during the 17 voyages from 1960 to 1982 and mapped the ice thickness distribution for the first time (Figure 2a). According to their results, the mean ice thickness above 65N is 2.9 m with a standard deviation of 1.8 m. This value was taken to be the standard “baseline” value for the Arctic Ocean before the recent thinning of the Arctic ice that has been reported (e.g. Rothrock et al., 1999).

In a further development of this method, Wadhams (1988) showed that additional information can be gained of the three-dimensional under-ice topography of Arctic ice using a side-scan sonar. Indeed, it was this technique that provided the first evidence for significant thinning of the Arctic ice cover over the past few decades (Wadhams, 1990; Rothrock et al., 1999; Tucker et al., 2001). By comparing the data obtained in 1958-1976 with those in the 1990s, Rothrock et al. (1999) showed that the mean ice draft at the end of the melt season decreased from 3.1 m to 1.8 m in the Arctic Ocean.

Despite all these pioneering results, the drawback to these data is that since this measurement is operated on a military basis, the observation is not necessarily systematic in space and time and time series of thickness data cannot be obtained within given areas (Wadhams, 2000). Therefore, it does not provide sufficient data sets to enable monitoring of change in ice thickness distribution on a seasonal or annual basis. Moreover, it cannot be applied to Antarctic ice because military submarines are prohibited from operating under Southern Ocean sea ice by the Antarctic Treaty.

## 2.2 Moored ice profiling sonar

This technique measures ice draft using a moored upward-looking sonar system which is tethered to a line attached to the seafloor. The principle is similar to that of submarine sonar. The device transmits a pulse of sound towards the surface, and the ice draft is then obtained by converting the travel time of the pulse to vertical distance allowing for variation in water temperature and pressure and subtracting it from the depth of the device (Figure 4). The footprint at the underside of the sea ice is about 2 m and the overall accuracy is 0.05 to 0.10 m (Melling and Riedel, 1995). The most remarkable merit of this method is that it can provide a time series of ice draft distribution at a fixed site with high temporal resolution (a few seconds to minutes) for several months. Thus it enables the monitoring of daily to seasonal variation in the ice draft distribution. Additionally, it can be deployed on the shallow continental shelf regions, where a submarine cannot operate. This is important because considerable deformation often occurs near the Arctic coastal region, to affect sub-sea ice exploration.

This technique was first applied to the near-shore region of the Beaufort Sea in the late 1970's (Hudson, 1990). From the over-winter measurements, the seasonal change of level ice thickness and the frequency of ridge keels were first revealed. In the same region, Melling and Riedel (1995, 1996) also deployed this system and examined the more detailed characteristics of deformed ice and under-ice topography by combining the ice motion obtained with a Doppler sonar. In Fram Strait, Vinje et al. (1998) examined the annual and seasonal variation of ice draft during the period of 1990 to 1996. By empirically converting ice draft to thickness and combining the ice drift data obtained from buoys, they estimated the annual mean ice volume flux through the Fram Strait to be  $2850 \text{ km}^3 \text{ yr}^{-1}$ . Combining this ice thickness data set with satellite-derived ice velocity Kwok and Rothrock (1999) found a relationship between the ice volume flux out of the central Arctic and the large-scale modes of atmospheric circulation (i.e. the North Atlantic Oscillation). In the Sea of Okhotsk, Marko (2003) applied this method to the east of Sakhalin Island and analyzed the ice draft data in conjunction with intense wave energy. Fukamachi et al. (2003, 2006) deployed this system in the coastal region of Hokkaido, Japan, and first revealed the ice thickness distribution including ridged ice in this region from three-year data sets.

In the Antarctic, where submarine sonar data are not available, this method has been an effective tool. However, it should be noted that there are some restrictions regarding deployment: the mooring system has to be operated from the seafloor at a depth deeper than 350-440 m to avoid ice bergs in the sea ice area (Massom et al., 2009), which may damage the instrument (Worby et al., 2001). Strass and Fahrbach (1998) examined the temporal and regional variation of ice draft across the Weddell Sea from six ice profiling sonars deployed between the tip of the Antarctic Peninsula and Kapp Norvegia from 1990 to 1994. Based on these data, Harms et al. (2001) estimated the annual mean ice volume export from the western Weddell Sea to be about  $0.05 \text{ Sv}$  ( $\sim 1580 \text{ km}^3 \text{ yr}^{-1}$ ). In East Antarctica, Worby et al. (2001) analyzed the seasonal variation of ice thickness distribution with this system.

Thus this method has significantly enhanced our knowledge of detailed ice thickness distribution, as a second tool to submarine sonar, for about three decades. It has allowed the estimation of various parameters related to ice thickness and in particular contributed to the understanding the fresh water budget through Fram Strait, which relates to, and has strong implications for climate change. Additionally, this method has enabled detection of ice ridge keels as deep as a few tens of meters (e.g. 29 m in the Beaufort Sea [Melling and Riedel, 1995] and 17 m in the Sea of Okhotsk [Fukamachi et al., 2006]). However, the drawback is that this device is not appropriate for obtaining the spatial distribution of ice thickness on a large scale at a given time, and has difficulties in monitoring ice thickness for more than decadal terms because of logistical constraints i.e. the need to recover and redeploy instruments every few years.

### 2.3 Video monitoring system

This technique is basically designed as a ship-based measurement. With a downward-looking video camera mounted on the side deck of a ship, ice conditions around the hull are continuously recorded along-track. Ice thickness is then estimated on the video images for ice floes which break up at the bow and turn into a side-up position alongside of the hull (Figure 5). The scale on the video image is determined by lowering a measured stick onto the ice surface while the ship is stationary. The reading error is less than a few centimetres. In

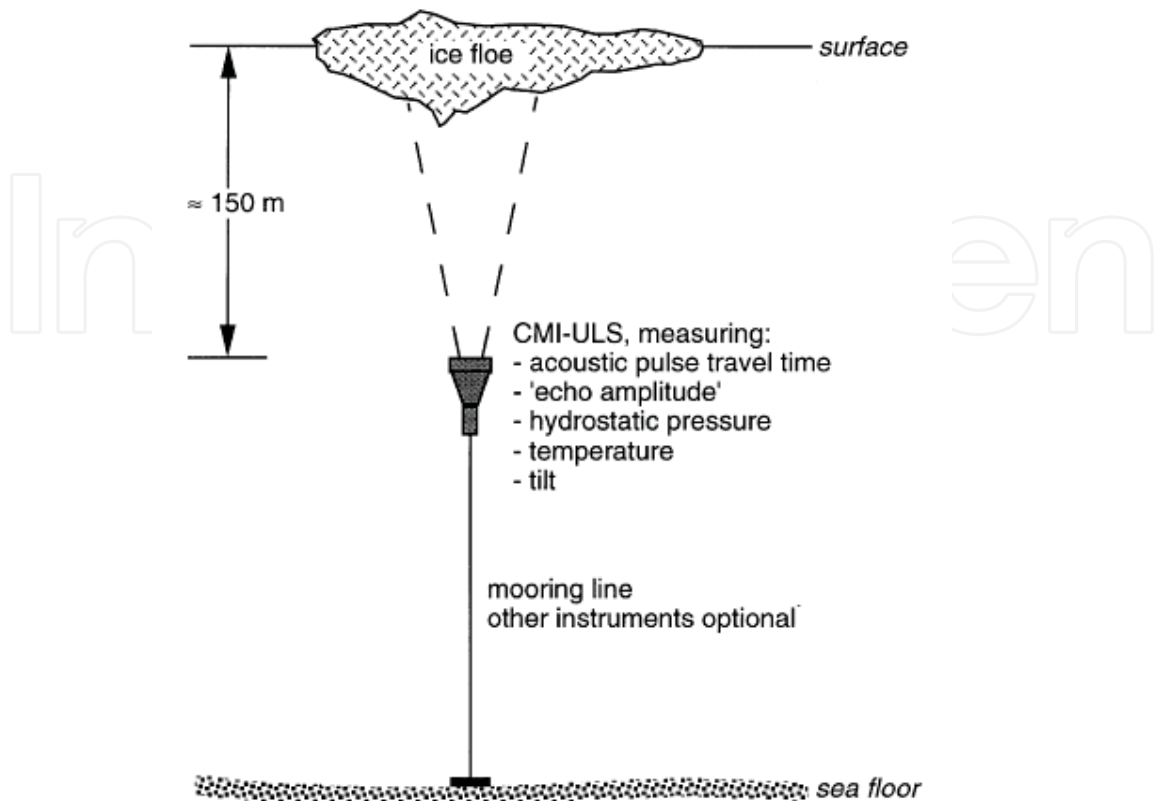


Fig. 4. Schematic representation of an ULS mooring set-up. (cited from Strass (1998))

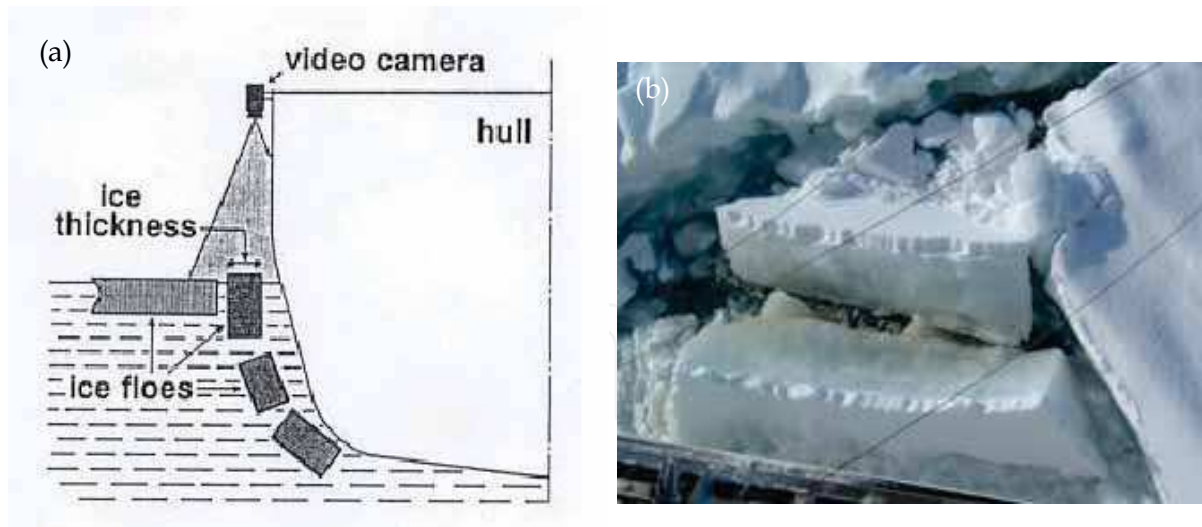


Fig. 5. Schematic picture of a video monitoring method.

(a) A schematic figure (cited from Shimoda et al. (1997))

(b) A typical picture of ice which was broken and turned into a side-up position. Note the brown color near the bottom, associated with the attachment of ice algae.



this way, spatial ice thickness distribution along the ship track can be determined in a relatively short amount of time. However, it should be noted that deformed ice, which is hard to turn, is beyond the measuring capability of this method, and that it is subject to the ship route which tends to be selected to traverse regions of thinner ice. These facts can cause some bias in the results i.e. a net underestimate in ice thickness distribution estimates. Therefore, this method is not appropriate for the measurement of thick ice distribution. This is in contrast with the measurement by upward-looking sonar, which is relatively free from such artificial bias.

Nevertheless, there are several advantages unique to this method. First, it is useful for obtaining the thickness distribution of level ice, accurate knowledge of which is important to understand the thermodynamic growth and rafting process (stacking of two ice floes without break-up). Secondly, it allows us to measure the overlying snow depth according to the degree of whiteness on the video images. This is particularly effective in the marginal ice zones, where ice is so thin that it is hard to measure snow depth directly. It also allows us to detect brown ice containing ice algae (Figure 5b). Thirdly, this system can be operated at a relatively low cost and does not require complicated calibration. Finally, without any risk of the damage by icebergs, this method can safely be applied in the coastal Antarctic ice area.

The key to this method is the downsizing of the video camera to facilitate its use. This system was first introduced to monitor the sea ice conditions in the Antarctic coastal region during the Japanese Antarctic Research Expeditions (JARE) in late 1980's (Shimoda et al., 1997). In this area, these observations were continued from 1988 to 2004, and from these results Uto et al. (2006a) found a significant annual variation in the thickness distribution of land-fast ice in the Lützow-Holm Bay near the Syowa Station and discussed the relationship with the break-up events of the land-fast ice there. This system was also deployed in the Sea of Okhotsk in 1991. Monitoring of the ice thickness distribution in the southern Sea of Okhotsk has continued since then from the icebreaker P/V "Soya", in collaboration with the Japan Coast Guard. Based on the data set obtained from 1991 to 2000, Toyota et al. (2004) showed that the thickness distribution follows a near Poisson distribution with an average of  $33 \pm 10$  cm, and proposed a stochastic rafting cycle model, referring to the layered structure. They also checked the accuracy of this method by comparing their data with the ice profiling sonar data obtained in that region (Fukamachi et al., 2003) and confirmed that the thickness distribution of these two methods matches well within the range of a few percent for non-ridged ice. Their group is still continuing these observations over this region, and the annual variations in mean ice thickness and volume are shown in Figure 6. In this figure, an annual variation in ice thickness is apparent with a period of about 7 years, while the trend towards a decrease in ice volume is remarkable, particularly after 2000.

In spite of several drawbacks, a video monitoring system therefore still remains an effective tool for obtaining ice thickness distributions, and in the marginal ice zones in particular. As this method provides direct measurements in a larger sense, it is sometimes used to validate the results of other remote sensing tools. However, the time-consuming task of analysing the images for measurement precludes real time monitoring and this problem should be improved on the computer base in the future.

## 2.4 Electromagnetic Induction Sounding

This device measures the distance from the instrument to the ice-seawater interface (i.e. ice bottom) using low-frequency (10 to 100 kHz) electromagnetic (EM) induction. The device is

composed of transmitter and receiver coils, which are set apart by a few meters. The transmitter generates a primary electromagnetic field which induces eddy currents mainly just below the ice bottom, because the conductivity of sea ice ( $0\text{--}50\text{ mS m}^{-1}$ ) is negligible compared to that of seawater ( $2500\text{ mS m}^{-1}$ ). In turn the induced currents generate a secondary electromagnetic field. Then the distance to the ice bottom is calculated from the strength of the secondary electromagnetic field sensed by the receiver coil. Therefore, if this device is used on the ice surface, the data obtained correspond directly to ice thickness. While the accuracy is  $\pm 0.1\text{ m}$  for undeformed ice, it degrades to up to 30 % for ridged ice because of the presence of seawater-filled cavities between the ice blocks and the smoothing effect caused by a larger footprint that is approximately equal to the distance to the ice bottom (Haas, 2003). Therefore validation is needed for ridged ice. The primary advantage of this method is that it allows us the measurement of ice thickness from the air, which is much easier than from below the ice. If we mount a laser profilometer on the instrument and measure the height of the instrument above the combined snow and ice surface, ice thickness can be obtained by subtracting it from the EM results and by incorporating knowledge of snow cover depth and density (Figure 7a). In this way, we can use an icebreaker or an aircraft to obtain profiles of ice thickness distribution with this device over a wide scale of 100s of kms. However, it should be noted that this method provides the summation of ice thickness and overlying snow depth. If we want to determine ice thickness itself, snow depth has to be measured by another tool and its density must also be factored in. Since this technique was first tested for the ground-based observations in the Arctic in the 1970's, numerous measurements were done to obtain ice thickness data in the various regions of the Arctic (Worby et al., 1999). The EM instrument used most frequently is the Geonics EM31 which contains the coils located at each end, 3.66 m apart (Figure 7b), and uses a frequency of 9.8 kHz. The ship-based EM system was first applied to the summer sea ice in the Bellingshausen and Amundsen Seas, Antarctica (Haas, 1998). This study found that the properties of summer ice, in particular seawater-filled gaps close to the ice surface, significantly reduces the accuracy of the EM measurement, although Worby et al. (1999) confirmed that the EM system is more robust when operating under winter and spring ice conditions in the Antarctic. The ship-based EM system was also introduced to the Sea of Okhotsk in 2004, where it was found that the seawater-filled cavities between the ice blocks in this region lower the accuracy of ice thickness estimates significantly, even in winter. Therefore, based on the calibration results from drilling on the ridged ice, Uto et al. (2006b) developed an algorithm that converts conductivity to ice thickness, taking into account the presence of gaps within the ice (Figure 8a). As a result, the measurement error was reduced to about 10 % for ridged ice, and the spatial ice thickness distribution, including ridged ice, was first revealed in this area. The comparison of ice thickness distribution with coincident ship-based video result in the same area is shown in Figure 8b, where reasonable agreement can be seen. However, the ground or ship-based EM measurement has a limitation in spatial coverage and may be biased according to the selection of ice floes or ship-route. For greater representativity, airborne measurement is desirable.

The airborne EM sounding technique was first developed with a helicopter in the Beaufort Sea in the mid 1980's (Kovacs et al., 1987; Kovacs and Holladay, 1989). Multala et al. (1996) subsequently applied the technique to Baltic Sea ice using a fixed-wing aircraft. By validating the data with drill-hole measurements, each study showed the method to be promising. Recently, the technique was developed further and improved using two

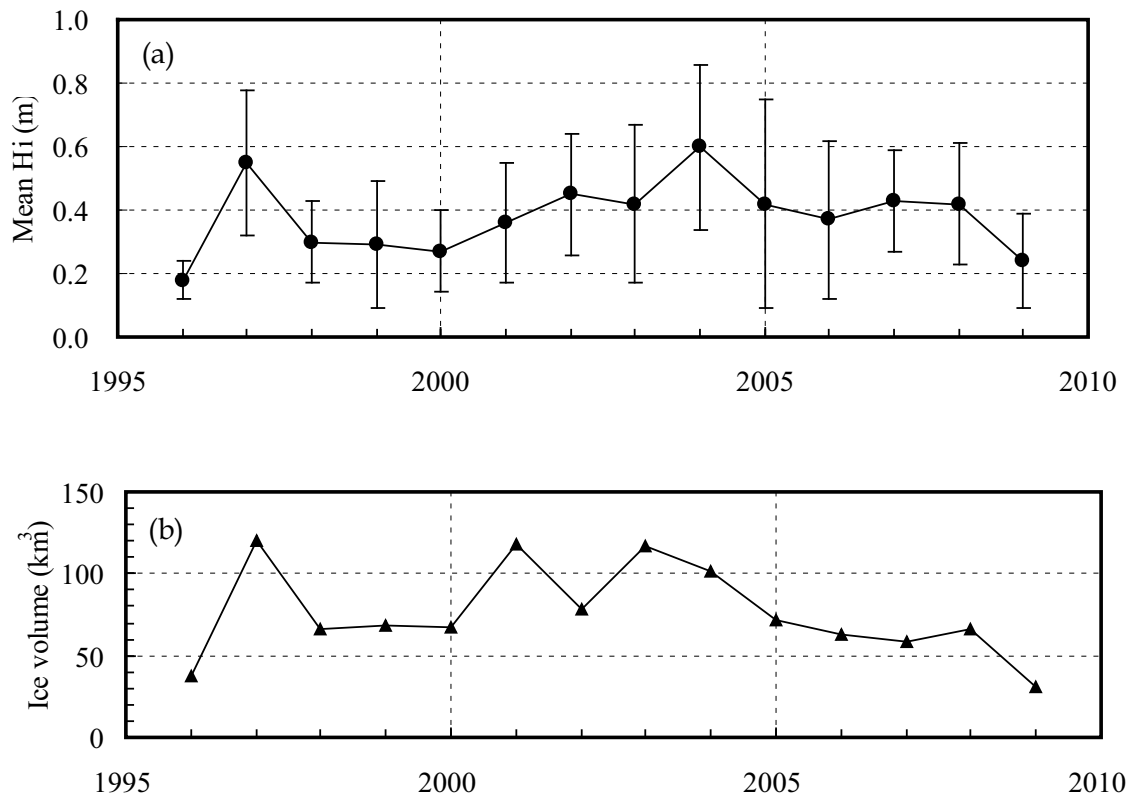


Fig. 6. Annual variations of (a) mean video thickness with a standard deviation (error bars) and (b) ice volume estimated by multiplying mean thickness and sea ice area in the southern Sea of Okhotsk, where sea ice area were offered by Japan Meteorological Agency.

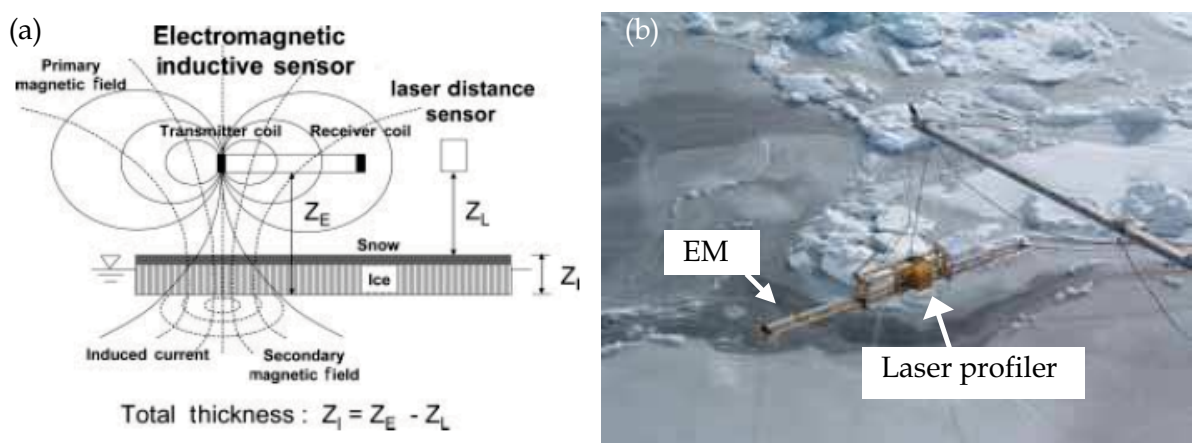


Fig. 7. Schematic picture of EM sounding system.

(a) Illustration of the principle of the measurement (cited from Uto et al. (2006b))

(b) A picture of EM set-up onboard the P/V "Soya" in the Sea of Okhotsk.

frequencies (3.7 and 112 kHz) for the systematic measurement, and since 2001 the monitoring and observation of ice thickness in the Arctic has been operated with a helicopter-borne EM by the German Alfred Wegener Institute for Polar and Marine Research (AWI). The details of the technique are described by Haas et al. (2009). By

combining this data set with the ground-based EM measurements acquired since 1991, Haas et al. (2008) showed a rapid thinning of sea ice had occurred in the Arctic Transpolar Drift in the 2000's and suggested a regime shift from multi-year to first-year ice.

Thus, the EM sounding technique has enabled us to remotely measure sea ice thickness from the air, which enhances the measurement considerably in comparison with the previous methods. With a ship- or helicopter-borne system, more detailed and spatial ice thickness distribution was revealed in various regions. Although a ship-based measurement may have some bias, it is effective especially in regions where relatively thin ice is dominant or helicopter operations are prohibited by law. However, it should be noted that it still needs validation, especially for melting ice or regions with significant ridges, and that its total areal coverage is rather limited.

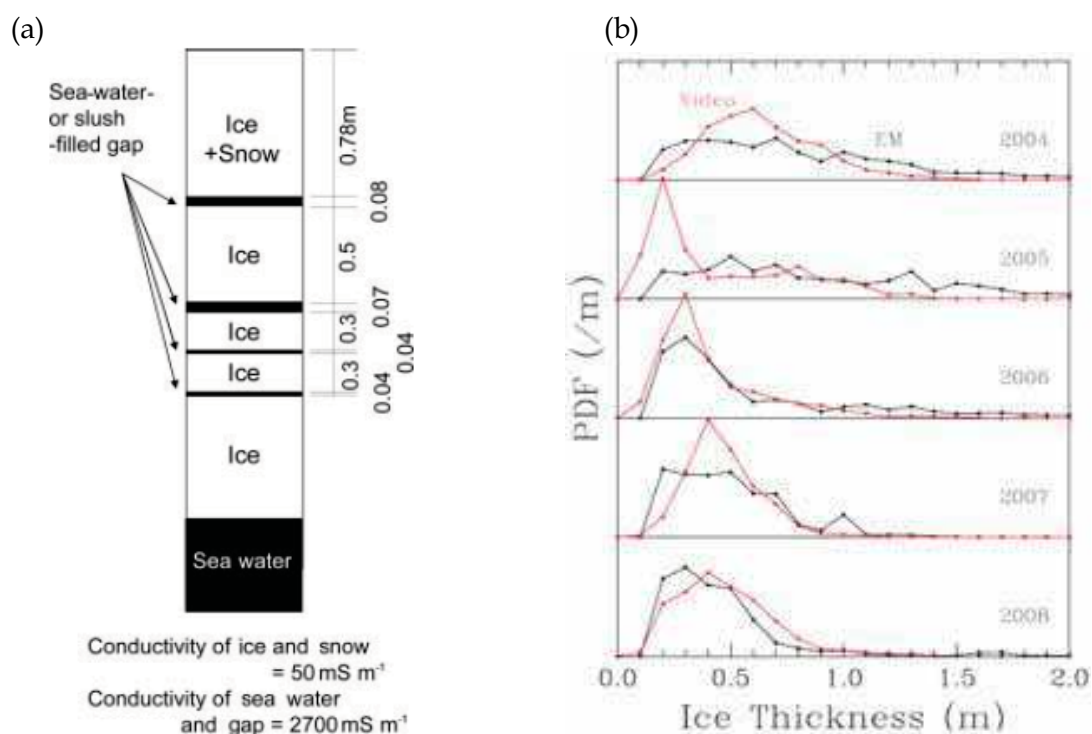


Fig. 8. (a) Model ice structure used for the algorithm converting conductivity to ice thickness developed for the Okhotsk ice. (cited from Uto et al. (2006b)). (b) Comparison of the probability density functions of ice thickness between the results obtained by converting the EM outputs to ice thickness with the algorithm (Figure 8a) and those obtained from video monitoring system in the Sea of Okhotsk during 2004 – 2008.

## 2.5 Satellite sensors

Previous sections have concentrated on various in-situ and airborne remote sensing tools. Although they have all contributed greatly to our knowledge about ice thickness distribution on a regional scale, ultimately it is the operational monitoring at a global scale via space-borne sensors that is most desirable. In this section, we evaluate the current situation regarding several satellite remote sensing possibilities.



### 2.5.1 Passive microwave methods

Multi-frequency passive microwave sensors have flown in space continuously since 1979. The merits of this sensor are: 1) the signal is not subject to the effect of cloud; 2) due to its large swath width, daily coverage is possible at a global scale; and 3) data can be obtained both day and night. Since the microwave emissivity of open water is much lower than that of sea ice, the areal coverage of sea ice can be derived with relatively high accuracy and thus several algorithms have been successfully developed to derive ice concentration using brightness temperature data acquired at the frequencies of 19 and 37 GHz (e.g. Cavalieri et al., 1984; Comiso, 1986). On the other hand, this has not necessarily been the case with ice thickness. Theoretically and from tank experiments, it has been shown that sea ice becomes opaque at all the microwave frequencies used at a thickness of less than a few centimetres (Troy et al., 1981; Grenfell and Comiso, 1986). Thus in a practical sense, the signals received by this sensor originate from the top few centimetres of sea ice and cannot include the direct information of ice thickness. Even so, if there are any surface dielectric properties of sea ice that do correlate well with ice thickness, they differentiate the emissivity and then allow the estimation of ice thickness. Fortunately, the dielectric properties depend on brine volume which is determined by salinity and temperature (Vant et al., 1978), and it is generally known that ice bulk salinity decreases with the increase of thickness through desalination over time by brine drainage and seasonal “flushing” by melt water (Kovacs, 1996). Furthermore, it was found for the Sea of Okhotsk ice that the surface brine volume fraction is highly correlated with ice thickness for ice thinner than 20 cm due to the multiplying effect of salinity and temperature (Figure 9). These observational results provide the physical grounds for the potential estimation of ice thickness with passive microwave sensors.

In the field, measurements of microwave emission over sea ice area were initiated using aircraft in the late 1960's (Wilheit et al., 1972). This was aimed at a preparation for the coming satellite observations, and they found that thin and thick ice can be discriminated at about 30 GHz due to the contrast in their emissivities at this frequency. Since the first scanning passive microwave sensor (Electrically Scanning Microwave Radiometer; 19.3 GHz) was flown on the Nimbus-5 in 1972, significant effort has been put into classifying sea ice types using passive microwave signals. The ESMR sensor was succeeded by the Scanning Multichannel Microwave Radiometer (SMMR) on Nimbus-7 (1978-1987), followed by the Special Sensor Microwave/Imager (SSM/I) on DMSP (1987-present) and the Advanced Microwave Scanning Radiometer-EOS (AMSR-E) since 2002. To interpret the satellite-derived data, the fundamental microwave properties of sea ice were studied from field experiments, and the dependence of emissivity on ice types and microwave frequencies was investigated in detail (Troy et al., 1981; Svendsen et al., 1983). As a result, it was revealed that while the microwave emissivity increases as sea ice grows from open water or nilas to first-year ice, it decreases to an intermediate value for Arctic multi-year ice, and that the difference in emissivity between ice types is large at frequencies below 40 GHz (Figure 10). Based on these results, Cavalieri (1994) succeeded in mapping ice type distribution in the Arctic Ocean, categorizing sea ice into nilas (< 10 cm thick), young (10-30 cm), first-year (> 30 cm), and multi-year ice with the SSM/I 19 and 37 GHz data. More recently, and from an aircraft campaign in the Sea of Okhotsk Naoki et al. (2008) showed



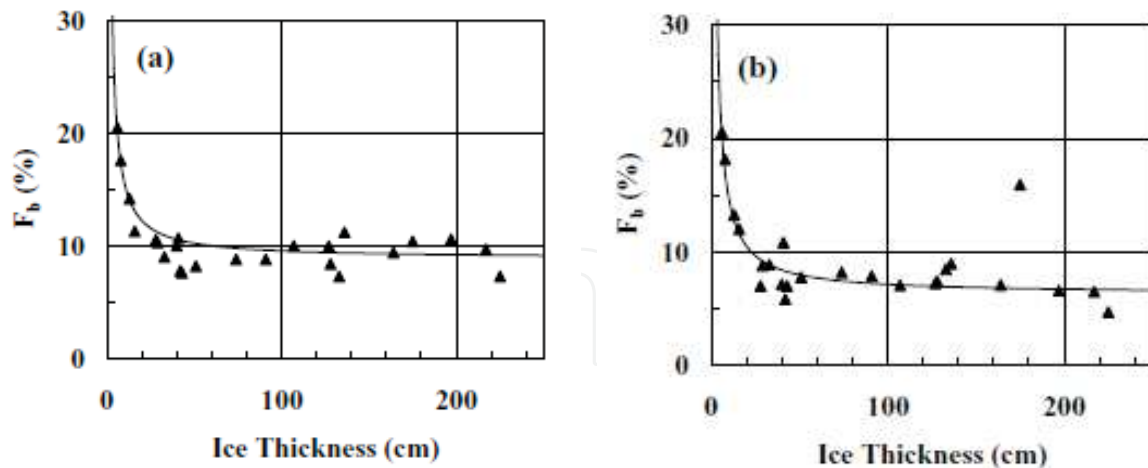


Fig. 9. Relationship between ice thickness and brine volume fraction for (a) bulk and (b) surface (top 9cm layer) mean for the Okhotsk ice. (from Toyota et al. (2007))

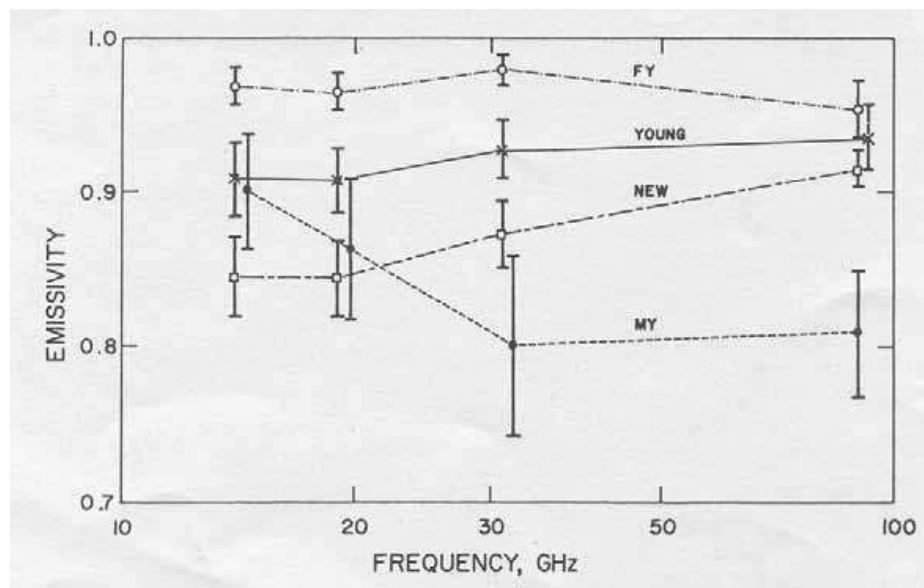


Fig. 10. Emissivity response curves in the 14 to 90 GHz range for four ice types. (cited from Troy et al. (1981))

that even the estimation of ice thickness for ice thinner 20 cm is possible with microwave data at 19 and 37 GHz. In fact, on the basis of the ice thickness calculated from AVHRR-derived ice surface temperature and a simple thermodynamic model, the algorithm which estimates the thin ice thickness ( $< 20$  cm) was successfully developed with SSM/I 37 GHz data for the Chukchi Sea (Martin et al., 2004) and with SSM/I 37 and 85 GHz data for the Antarctic (Tamura et al., 2007). Martin et al. (2005) further extended the analysis using AMSR-E data for the Chukchi Sea. In addition to the four thickness categories, Tateyama et al. (2002) and Tamura et al. (2007) proposed the use of the 85 GHz data to detect fast ice area. In summary it is concluded that passive microwave data can be usefully used to estimate ice thickness distribution for ice thinner than 20 cm. This is important because it is over the thin

ice area that the most intense heat exchange between ocean and atmosphere occurs in winter (Maykut, 1978), producing high rates of brine rejection from growing ice and dense water formation. With SSM/I-derived ice thickness information, Tamura et al. (2008) mapped the amount of ice production around the Antarctic coast and discussed the geographical features. However, it should be noted that the spatial resolution is rather coarse (25 km for SSM/I 37 GHz data) and that at present this method is available only for ice at an early stage of growth. It has not been guaranteed for deformed ice or snow-covered ice yet because surface roughness or snow also has significant influence on the emissivity (Grenfell and Comiso, 1986; Brown and Armstrong, 2008). For such ice conditions, further studies are needed.

### 2.5.2 Active microwave methods

The key merit of this sensor is, as with passive microwave, that it is available irrespective of either cloud or darkness. In addition, the advent of space-borne Synthetic Aperture Radar (SAR) has made it possible to obtain the backscatter coefficient data with a horizontal resolution of 10 to 100 m, although the swath width is limited to a few tens to hundreds of kilometres. In general, the backscatter coefficient includes the effects of both surface scattering and volume scattering, depending on the microwave frequency and ice conditions such as salinity, roughness (degree of deformation) and temperature. Snow cover tends to be largely transparent unless wet. For typical first-year ice with a salinity of 5 psu at a temperature of -5 deg. C, the penetration depth of the microwaves is only about 10 cm at the C-band (Hallikainen and Winebrenner, 1992). Therefore, the backscatter coefficient is predominantly determined from surface scattering for first-year ice. Since the surface scattering includes the effects of both the dielectric properties of the top layer and the surface roughness of the ice, the principle of the method is to relate either of these two parameters to ice thickness. As mentioned in the previous section, the former is well correlated with ice thickness for ice thinner than 20 cm. Therefore if these two effects can be separated, the estimation of ice thickness distribution becomes possible for thin ice. Fortunately, it was found that the effect of surface roughness can be reduced by taking the ratio of the VV (vertical) to HH (horizontal) backscattering (Winebrenner et al., 1989). In fact, from field experiments using an airborne L-band SAR in the Sea of Okhotsk, it was revealed that the VV-HH ratio is well correlated with ice thickness for relatively thin ice (Figure 11; Wakabayashi et al., 2004; Nakamura et al., 2005). Thus, it was confirmed that polarimetric data are particularly useful as a means of remotely estimating thin ice thickness distribution in the peripheral Arctic seas.

Then what about thick ice distribution? Toyota et al. (2009) presented the usefulness of L-band SAR backscattering to estimate thick ice thickness distribution in the SSIZ from the airborne Pi-SAR campaign in the Sea of Okhotsk. The main results and conclusions of this work will be summarized here.

It is generally known that in the SSIZ ridging (pile-up) activities are a key process by which the ice thickens (e.g. Worby et al., 1996; Toyota et al., 2007). It follows therefore that the degree of surface roughness correlates with ice thickness. As discussed by Dierking and Busche (2006), L-band SAR data (wavelength = 24 cm) seem more suitable for this purpose than C-band (6 cm) data. This is because the longer wavelength approximates the horizontal

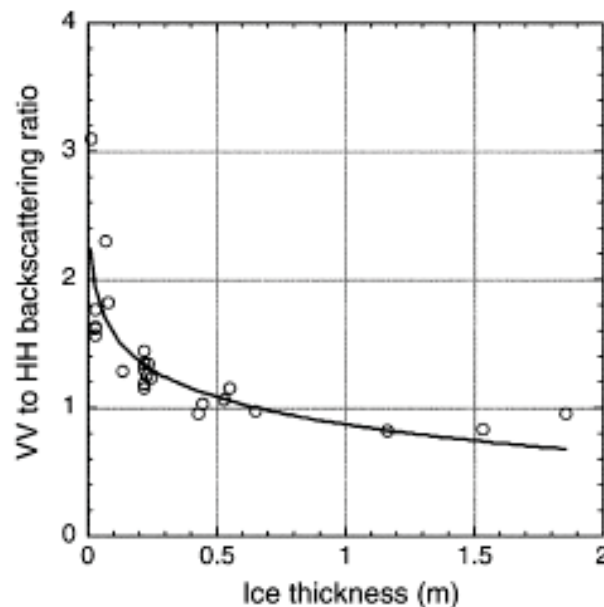


Fig. 11. Relations between ice thickness and VV-to-HH backscattering ratio obtained from airborne L-band SAR in the Sea of Okhotsk. (cited from Wakabayashi et al. (2004))

roughness scale of the ice surface more closely (Massom, 2006). Spaceborne L-band SARs have been launched on JERS-1 and ALOS, while C-band instruments have flown on ERS-1 and -2, Radarsat-1 and -2 and Envisat. Details are given in Lubin and Massom (2006).

To verify this idea, Toyota et al. (2009) conducted ship-borne electromagnetic (EM) induction sounding and supersonic profiling observations with an icebreaker, coordinated with airborne L-band SAR observations in the southern Sea of Okhotsk in February 2005 (Figure 12). The general conditions of ice thickness in the study area were of undeformed ice thickness ranging from 0.3 to 0.7 m with an average of 0.33 m, and a total average ice thickness, including ridged ice area fraction (26%), was estimated to be 0.84 m. The surface elevation was estimated with a supersonic profiler by representing the ship's motion with a low-pass filter.

Based on results obtained along a 40 km observation line, radar backscattering coefficients correlated well with ice thickness (correlation coefficient = 0.88) and surface roughness (i.e. 0.80), defined by the standard deviation of surface elevation (Figure 13abc). Here, it should be noted that the theoretical microwave penetration depth is up to 0.50 m at L-band for first-year ice with a salinity of 5.1 psu (Hallikainen and Winebrenner, 1992). Therefore, backscattering is affected by the internal structure of the sea ice, which should work to decrease the correlation with ice thickness. Importantly and in spite of this property, the L-band backscatter coefficient corresponds well with surface roughness. On the other hand, the VV-HH ratio has a lower correlation with ice thickness (i.e. -0.77) than either VV or HH (Figure 13d). This means that backscatter coefficients are useful for estimating the thickness distribution for thick ice not through the dielectric properties but through roughness properties. All these results shed light on the possibility for determining ice thickness distribution in SSIZ from polarimetric radar backscatter data.

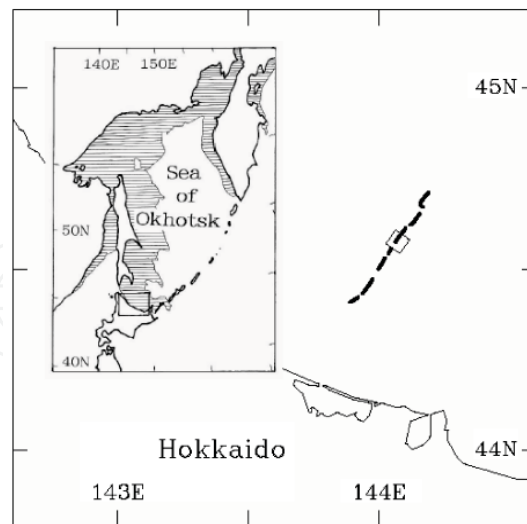


Fig. 12. Location map of the Pi-SAR experiment conducted in mid-February 2005 in the Sea of Okhotsk. Solid lines denote the observation line selected for analysis. (cited from Toyota et al. (2009))

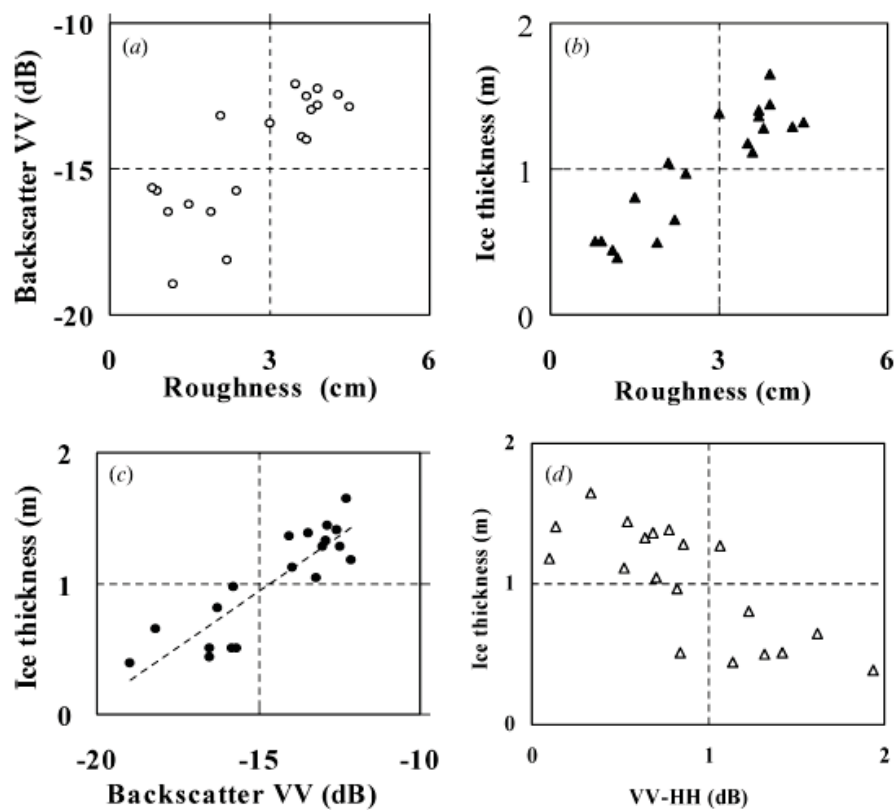


Fig. 13. Scatter plots of the 1 km-averaged values between (a) surface roughness and Backscatter coefficient (VV), (b) surface roughness and ice thickness, (c) backscatter coefficient (VV) and ice thickness, (d) backscattering ratio (VV-HH) and ice thickness. (cited from Toyota et al. (2009))

In summary, ice thickness retrieval for first-year ice by L-band SAR is promising for a wide range of ice thickness by virtue of the effect on the dielectric constant of surface properties for relatively thin undeformed ice and of surface roughness for thicker ice. On the other hand, multi-year ice has significantly different properties in the Arctic in particular. Due to desalination in summer, the penetration depth becomes deeper for Arctic multi-year sea ice, and then the volume scattering becomes more significant at L-band. In this case, C-band is more appropriate to distinguish between multi-year ice and deformed first-year ice (Rignot and Drinkwater, 1994). Therefore, as pointed out by Rignot and Drinkwater (1994), ultimately the combining of C- and L-band is optimal for the overall classification of ice types. Since the L-band data are now available from the ALOS/PALSAR with polarimetric and ScanSAR modes, combined analysis with C- and L-band is expected in the near future.

### 2.5.3 Altimeter methods

This sensor measures the freeboard of sea ice (i.e. its height relative to sea level), and freeboard is then converted to ice thickness by assuming that a floating ice floe is in isostatic balance. At present there are two kinds of altimeters available for this type of ice thickness estimation: radar and Laser profiler. Radar altimeters operating at a frequency of 13.8 GHz on the ERS-1 and ERS-2 satellites were launched in 1991 and 1995, respectively. The coverage area for these data extends to 81.5°N and S with a footprint of ~1 km. Since it has been confirmed from the laboratory experiments that reflected echoes come from the interface between sea ice and snow (Beaven et al., 1995), this sensor basically measures the height of snow/ice interface relative to sea level with an accuracy of 10 cm. The relatively large footprint limits the applicable area to closely packed ice area, however the key advantage remains that the data can be obtained irrespective of weather conditions, albeit along a profile. Conversely, the laser altimeter (Geoscience Laser Altimeter System or GLAS) onboard ICESat satellite, launched in January 2003, operates at a wavelength of 1064 nm and covers the area up to 86°N and S. In this case, the sensor measures the elevation of the ice or snow surface within a footprint of 70 m spaced at 170 m and an overall accuracy of 14 cm (Kwok and Cunningham, 2008). Although such a small footprint promises detailed analysis, it should be noted that this sensor is subject to cloud contamination, which may be critical for the polar research, as pointed by Haas (2003). A schematic figure is shown in Figure 14 and the calculation for each sensor is as below:

$$\text{Radar: } h_i = \frac{\rho_w}{\rho_w - \rho_i} h_f + \frac{\rho_s}{\rho_w - \rho_i} h_s \quad (1)$$

and

$$\text{Laser: } h_i = \frac{\rho_w}{\rho_w - \rho_i} h_{ts} - \frac{\rho_w - \rho_s}{\rho_w - \rho_i} h_s \quad (2)$$

, where  $\rho_i$ ,  $\rho_s$ , and  $\rho_w$  are the densities of sea ice, snow and seawater, respectively, and the notation of  $h$  is given in Figure 14. For both altimeters, the key need is to estimate the reference sea level, and to incorporate accurate estimates of the density of seawater, snow and sea ice, and the snow depth.



This method was first applied in the Arctic Ocean by Laxon et al. (2003), using the ERS radar altimeter. In this case, the reference sea level was analyzed using individual echoes with some corrections for orbits, tides, and atmospheric pressure (Peacock and Laxon, 2004),

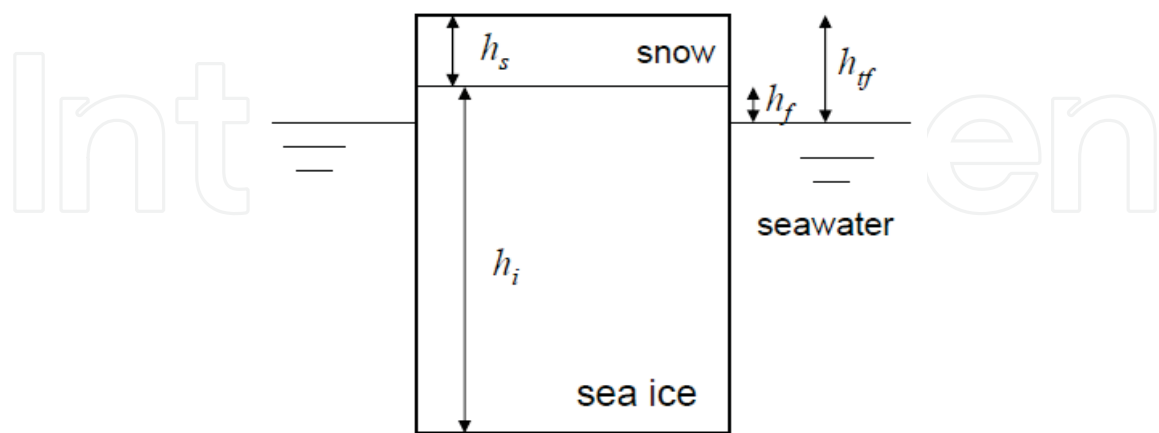


Fig. 14. Schematic picture showing the variables of snow depth ( $h_s$ ), ice thickness ( $h_i$ ), ice freeboard ( $h_{if}$ ), and total freeboard ( $h_{tf}$ ).

and the density of sea ice and seawater was assumed to be constant (i.e. 915 and 1024 kg m<sup>-3</sup>). The density and depth of snow were taken from a monthly climatology. Submarine sonar data were used for validation of the ice thickness product. As a result, the authors succeeded in extracting the geographical distribution of the Arctic ice thickness and showed the availability of this method for ice thicker than 1 m. Furthermore and on the basis of an 8-year data set (1993-2001), they found out that the interannual variation is much larger than predicted by numerical models, and that this large variability could be better explained by the length of melting season than expected changes of atmospheric and oceanic circulation. Similarly the results from the algorithm used by the ICESat GLAS laser altimeter has recently been analyzed by Kwok et al. (2004), Kwok & Cunningham (2008) to the Arctic Ocean, and by Zwally et al. (2008) in the Weddell Sea. Kwok & Cunningham (2008) used the ECMWF outputs for snow data, and tested two cases of sea ice density as a constant value (925 kg m<sup>-3</sup>) and a function of ice thickness, while Zwally et al. (2008) used AMSR-derived snow depth and constant densities for snow (300 kg m<sup>-3</sup>) and sea ice (915 kg m<sup>-3</sup>). The method for estimating the reference sea level was developed individually. As a result, these studies all succeeded in showing the potential usefulness of this method. However, as mentioned by both of the authors, the improved knowledge about snow is crucial because of the sensitivity of laser altimetry to the temporal variation of snow depth and density.

In summary, it has been shown that satellite altimeters are useful as a means of estimating ice thickness distributions over a wide scale, and for thick ice in particular. The primary merit is the ability to obtain hemispheric ice thickness distribution on a seasonal time scale, which allows us to monitor trends in ice thickness change and validate the results from numerical models. In turn, this will feed back to an improvement in the way dynamical processes are prescribed in the sea ice models. However, it should also be noted that improved knowledge about densities of snow and sea ice is still needed for this method, since observational data show that they range widely and also evolve over time according to

the meteorological conditions. In addition, we need to consider the effect of the seawater-filled cavities between ice blocks on the altimeter estimates. Since such cavities increase the bulk ice density, the further investigation will be needed. An additional concern relates to the footprint size. Since this method is based on the assumption of isostatic balance, research needs to be carried out to determine whether the important underlying assumption of isostatic balance holds at the scale of the footprints.

### 3. Concluding Remarks

In this chapter, a brief history of ice thickness measurement has been presented, stressing how remote sensing tools have contributed to an improved understanding of the sea ice thickness distribution and its importance in sea ice research. Since Weyprecht first conducted the observation of the ice thickness growth at the Franz-Joseph Island (80°N) during the 1873/74 winter (Zubov, 1945), ice thickness has been one of the most challenging and interesting topics in sea ice research. As seen above, in general the tools have been developed to cover a wider region. Most recently satellite altimeters have allowed us to monitor the ice thickness distribution at a hemispheric scale and on a seasonal time scale, albeit limited to thick ice. Since the response of sea ice associated with recent global warming receives much attention now, it is a notable achievement to be able to discuss the ice thickness trends not only from the products of numerical models but also on the basis of observational results. This will also be helpful for the improvement of physical processes in the models, and validation of their output.

In spite of these advances, it is unlikely that all of the various methods developed to date will be replaced by satellite sensors. The individual tools are appropriate for measurement at their optimum scale. In general, ice thickness varies in a hierarchical fashion, as suggested by Rothrock and Thorndike (1980), and the properties at each scale have an influence on those at a different scale. For example, the ice thickness distribution at a scale of a few to tens of meters is directly involved in the formation of ridges, while it is the thickness properties at a scale of a few kilometres that determine the external forcing for ridging. Thus, a more comprehensive understanding of sea ice behaviours depends upon acquisition of accurate information on the ice thickness distribution at both local and large scales. Considering that ice formation and melting are basically localized processes, the interaction between different scales needs to be further clarified when using the different though complementary tools at different scale; this factor will become more important to the sea ice research in the future.

It should be mentioned that there are other methods widely used for ice thickness measurement. The representative one is visual observation on the basis of ASPeCT protocol, which was designed for the ship-based observations in the Antarctic seas by Australian researchers based on a previous method used by other groups in the 1980's (Worby & Allison, 1999). The observation is conducted every hour from the ship's bridge along-track, including the thickness of sea ice and snow, floe size, and surface properties. Although there may be some problems with accuracy and bias from the ship-track, this is a convenient method and the statistics obtained represent useful general characteristics of the ice cover. A climatology of sea ice thickness obtained in this fashion are presented in Figure 1.2b. The continuation of this type of observing program is to be encouraged.

Finally, I would like to close this chapter by concluding that the history of ice thickness

measurement is closely related to the development of sea ice research on both macro- and micro- scale properties, and that many researchers from a variety of backgrounds have been involved in it. Therefore, this is truly an interdisciplinary issue, and further collaboration with many researches is highly desirable in future.

#### 4. Acknowledgments

The author expresses his sincere gratitude to Dr. Robert Massom (Antarctic Climate and Ecosystems Cooperative Research Centre and Australian Antarctic Division) for the critical reading of this manuscript and valuable comments and to Dr. Guy Williams (Hokkaido Univ.) for the proof-reading. They are very helpful for the improvement of the manuscript.

#### 5. References

- Ackley, S.F. (1979). Mass-balance aspects of Weddell Sea pack ice, *J. Glaciol.*, Vol. 24, No.90, pp. 391-405.
- Beaven, S.G.; Lockhart, G.L.; Gogineni, S.P.; Hossetnmostafa, A.R.; Jezek, K.; Gow, A.J.; Perovich, D.K.; Fung, A.K. & Tjuatja, S. (1995). Laboratory measurements of radar backscatter from bare and snow-covered saline ice sheets, *Int. J. Remote Sens.*, Vol. 16, No. 5, pp. 851-876.
- Bourke, R.H. & Garrett, R.P. (1987). Sea ice thickness distribution in the Arctic Ocean, *Cold Regions Science and Technology*, Vol.13, pp.259-280.
- Brown, R. & Armstrong, R.L. (2008). Snow-cover data: measurement, products, and sources, In *Snow and Climate*, Armstrong, R.L. & Brun, E. (ed.), pp. 181-216, Cambridge University Press, ISBN 978-0-521-85454-2, Cambridge, UK.
- Cavalieri, D.J.; Gloersen, P. & Campbell, W.J. (1984). Determination of sea ice parameters with the NIMBUS 7 SMMR, *J. Geophys. Res.*, Vol. 89, No.D4, pp. 5355-5369.
- Cavalieri, D.J. (1994). A microwave technique for mapping thin sea ice, *J. Geophys. Res.*, Vol.99, No.C6, pp. 12561-12572.
- Comiso, J.C. (1986). Characteristics of Arctic winter sea ice from satellite multispectral microwave observation, *J. Geophys. Res.*, Vol.91, No.C1, pp.975-994.
- Dierking, W. & Busche, T. (2006). Sea ice monitoring by L-band SAR: An assessment based on literature and comparisons of JERS-1 and ERS-1 imagery, *IEEE Trans. Geosci. Remote Sensing*, Vol. 44, No.2, pp. 957-970.
- Fukamachi, Y.; Mizuta, G.; Ohshima, K.I.; Melling, H.; Fissel, D. & Wakatsuchi, M. (2003). Variability of sea-ice draft off Hokkaido in the Sea of Okhotsk revealed by a moored ice-profiling sonar in winter of 1999, *Geophys. Res. Lett.*, Vol.30, No.7, 1376, doi:10.1029/2002GL016197.
- Fukamachi, Y.; Mizuta, G.; Ohshima, K.I.; Toyota, T.; Kimura, N. & Wakatsuchi, M. (2006). Sea ice thickness in the southwestern Sea of Okhotsk revealed by a moored ice-profiling sonar, *J. Geophys. Res.*, Vol.111, C09018, doi:10.1029/2005JC003327.
- Gow, A.J.; Ackley, S.F.; Weeks, W.F. & Govoni, J.W. (1982). Physical and structural characteristics of Antarctic sea ice, *Ann. Glaciol.*, Vol.3, pp.113-117.
- Grenfell, T.C. & Comiso, J.C. (1986). Multifrequency passive microwave observations of first-year sea ice grown in a tank, *IEEE Trans. Geosci. Remote Sensing*, Vol.GE-24, No.6, pp. 826-831.

- Haas, C. (1998). Evaluation of ship-based electromagnetic-inductive thickness measurements of summer sea-ice in the Bellingshausen and Amundsen Seas, Antarctica, *Cold Reg. Sci. Technol.*, Vol. 27, pp. 1-16.
- Haas, C. (2003). Dynamics versus thermodynamics: The sea ice thickness distribution, In *Sea Ice*, Thomas, D.N. & Dieckmann, G.S. (Ed.), pp. 82-111, Blackwell Publishing, ISBN 0-632-05808-0, Oxford, U.K.
- Haas, C.; Pfaffling, A.; Hendricks, S.; Rabenstein, L.; Etienne, J.-L. & Rigor, I. (2008). Reduced ice thickness in Arctic Transpolar Drift favors rapid ice retreat, *Geophys. Res. Lett.*, Vol.35, L17501, doi:10.1029/2008GL034457.
- Haas, C.; Lobach, J.; Hendricks, S.; Rabenstein, L. & Pfaffling, A. (2009). Helicopter-borne measurements of sea ice thickness, using a small and lightweight, digital EM system, *J. Appl. Geophys.*, Vol.67, pp.234-241.
- Hallikainen, M. & Winebrenner, D.P. (1992). The physical basis for sea ice remote sensing, In *Microwave Remote Sensing of Sea Ice*, Carsey (ed.), pp. 29-46, American Geophysical Union, Washington D.C.
- Harms, S.; Fahrbach, E. & Strass, V.H. (2001). Sea ice transports in the Weddell Sea, *J. Geophys. Res.*, Vol.106, No.C5, pp. 9057-9074.
- Hudson, R. (1990). Annual measurement of sea-ice thickness using an upward-looking sonar, *Nature*, Vol.344, pp.135-137.
- Japan Meteorological Agency (2005). *The Results of Sea Ice Observations*, Vol. 23, (2004-2005). (CD-ROM)
- Kovacs, A.; Valleau, N.C. & Holladay, J.S. (1987). Airborne electromagnetic soundings of sea ice thickness and sub-ice bathymetry, *Cold Reg. Sci. Technol.*, Vol.14, pp. 289-311.
- Kovacs, A. & Holladay, J.S. (1989). Development of an airborne sea ice thickness measurement system and field test results, *CRREL Report*, Vol.89-19, pp. 1-47.
- Kovacs, A. (1996). Sea Ice. Part I. Bulk salinity versus ice floe thickness. *USA Cold Regions Research and Engineering Laboratory, CRREL Rep.*, Vol.97-7, pp. 1-16.
- Kwok, R. & Rothrock, D.A. (1999). Variability of Fram Strait ice flux and North Atlantic Oscillation, *J. Geophys. Res.*, Vol.104, No.C3, pp.5177-5189.
- Kwok, R.; Zwally, H.J. & Yi, D. (2004). ICESat observations of Arctic sea ice: First look, *Geophys. Res. Lett.*, Vol. 31, L16401, doi:10.1029/2004GL020309.
- Kwok, R. & Cunningham, G.F. (2008). ICESat over Arctic sea ice: Estimation of snow depth and ice thickness, *J. Geophys. Res.*, Vol. 113, C08010, doi:10.1029/2008JC004753.
- Lange, M.A. & Eicken, H. (1991). Textural characteristics of sea ice and the major mechanism of ice growth in the Weddell Sea, *Ann. Glaciol.*, Vol. 15, pp. 210-215.
- Laxon, S.; Peacock, N. & Smith, D. (2003). High interannual variability of sea ice in the Arctic region, *Nature*, Vol. 425, pp. 947-950.
- Lubin, D. & Massom, R. (2006). *Polar Remote Sensing, Volume 1: Atmosphere and Oceans*, Praxis Publishing Ltd and Springer, ISBN 3-540-43097-0, Chichester, UK and Berlin, Germany.
- Marko, J.R. (2003). Observation and analyses of an intense wave-in-ice event in the Sea of Okhotsk, *J. Geophys. Res.*, Vol.108, No.C9, 3296, doi:10.1029/2001JC001214.
- Martin, S.; Drucker, R.; Kwok, R. & Holt, B. (2004). Estimation of the thin ice thickness and heat flux for the Chukchi Sea Alaskan coast polynya from Special Sensor Microwave/Imager data, 1990-2001, *J. Geophys. Res.*, Vol. 109, No.C10012, doi: 10.1029/2004JC002428.



- Martin, S.; Drucker, R.; Kwok, R. & Holt, B. (2005). Improvements in the estimates of ice thickness and production in the Chukchi Sea polynyas derived from AMSR-E, *Geophys. Res. Lett.*, Vol. 32, L05505, doi:10.1029/2004GL022013.
- Massom, R. (2006). Basic remote-sensing principles relating to the measurement of sea ice and its snow cover, In *Polar Remote Sensing Vol. I: Atmosphere and Oceans*, Lubin, D. & Massom, R. (ed.), pp. 356-380, Praxis Publishing Ltd, ISBN 3-540-43097-0, Chichester, UK and Berlin, Germany, 756 pp.
- Massom, R.; Hill, K.; Barbraud, C.; Adams, N.; Ancel, A.; Emmerson, L. & Pook, M.J. (2009). Fast ice distribution in Adelie Land, East Antarctica: Interannual variability and implications for emperor penguins (*Aptenodytes forsteri*), *Marine Ecol. Progr. Ser.*, Vol. 374, pp. 243-257.
- Maykut, G.A. (1978). Energy exchange over young sea ice in the central Arctic, *J. Geophys. Res.*, Vol. 83, No.C7, pp. 3646- 3658.
- McLaren, A.S. (1989). The under-ice thickness distribution of the Arctic Basin as recorded in 1958 and 1970, *J. Geophys. Res.*, Vol.94, No.C4, pp. 4971-4983.
- Melling, H. & Riedel, D.A. (1995). The underside topography of sea ice over the continental shelf of the Bering Sea in the winter of 1990, *J. Geophys. Res.*, Vol.100, No.C7, pp.13641-13653.
- Melling, H. & Riedel, D.A. (1996). Development of seasonal pack ice in the Beaufort Sea during the winter of 1991-1992: a view from below, *J. Geophys. Res.*, Vol.101, No.C5, pp.11975-11991.
- Multala, J.; Hautaniemi, H.; Oksama, M.; Lepparanra, M.; Haapala, J.; Herlevi, A.; Riska, K. & Lensu, M. (1996). An airborne electromagnetic system on a fixed wing aircraft for sea ice thickness mapping, *Cold Reg. Sci. Technol.*, Vol.24, pp.355-373.
- Nakamura, K.; Wakabayashi, H.; Naoki, K.; Nishio, F.; Moriyama, T. & Uratsuka, S. (2005). Observation of sea ice thickness in the Sea of Okhotsk by using dual-frequency and fully polarimetric airborne SAR (Pi-SAR) data, *IEEE Trans. Geosci. Remote Sensing*, Vol. 43, 2460-2469.
- Naoki, K.; Ukita, J.; Nishio, F.; Nakayama, M.; Comiso, J.C. & Gasiewski, Al (2008). Thin sea ice thickness as inferred from passive microwave and in situ observations, *J. Geophys. Res.*, Vol. 113, No.C02S16, doi:10.1029/2007JC004270.
- Nghiem, S.V.; Rigor, I.G.; Perovich, D.K.; Clemente-Colon, P.; Weatherly, J.W. & Neumann, G. (2007). Rapid reduction of Arctic perennial sea ice, *Geophys. Res. Lett.*, Vol. 34, L19504, doi:10.1029/2007GL031138.
- Peacock, N.R. & Laxon, S.W. (2004). Sea surface height determination in the Arctic Ocean from ERS altimetry, *J. Geophys. Res.*, Vol. 109, C07001, doi:10.1029/2001JC001026.
- Rignot, E. & Drinkwater, M.R. (1994). Winter sea-ice mapping from multi-parameter synthetic-aperture radar data, *J. Glaciol.*, Vol. 40, No. 134, pp. 31-45.
- Rothrock, D.A. & Thorndike, A.S. (1980). Geometric properties of the underside of sea ice, *J. Geophys. Res.*, Vol. 85, No. C7, pp. 3955-3963.
- Rothrock, D.A. (1986). Ice thickness distribution – measurement and theory. In: *The Geophysics of Sea Ice* (ed. N. Untersteiner), Plenum, New York, pp. 551-575.
- Rothrock, D.A.; Yu, Y. & Maykut, G.A. (1999). Thinning of the Arctic sea-ice cover. *Geophys. Res. Lett.*, Vol.26, No.23, pp. 3469-3472.
- Shimoda, H.; Endoh, T.; Muramoto, K.; Ono, N.; Takizawa, T.; Ushio, S.; Kawamura, T. & Ohshima, K.I. (1997). Observations of sea-ice conditions in the Antarctic coastal



- region using ship-board video cameras, *Antarctic Record*, Vol.41, No.1, pp.355-365. (in Japanese with English summary)
- Strass, V.H. (1998). Measuring sea ice draft and coverage with moored upward looking sonars, *Deep-Sea Res. I*, Vol.45, 795-818.
- Strass, V.H. & Fahrbach, E. (1998). Temporal and regional variation of sea ice draft and coverage in the Weddell Sea obtained from upward looking sonars, In: *Antarctic Sea Ice, Physical Processes, Interactions and Variability*, Jeffries, M.O. (Ed.), pp.123-139, American Geophysical Union, ISBN 0-87590-902-7, Washington, D.C.
- Svendsen, E.; Kloster, K.; Farrelly, B.; Johanessen, O.M.; Johanessen, J.A.; Campbell, W.J.; Gloersen, P.; Cavalieri, D.J. & Matzler, C. (1983). Norwegian remote sensing experiment: evaluation of the Nimbus 7 scanning multichannel microwave radiometer for sea ice research, *J. Geophys. Res.*, Vol.88, No.C5, pp. 2781-2792.
- Tamura, T.; Ohshima, K.I.; Markus, T.; Cavalieri, D.J.; Nihashi, S. & Hirasawa, N. (2007). Estimation of thin ice thickness and detection of fast ice from SSM/I data in the Antarctic Ocean, *J. Atmos. Ocean. Tech.*, Vol. 24, pp.1757-1772.
- Tamura, T.; Ohshima, K.I. & Nihashi, S. (2008). Mapping of sea ice production for Antarctic coastal polynyas, *Geophys. Res. Lett.*, Vol.35, No.L07606, doi:10.1029/2007GL032903.
- Tateyama, K.; Enomoto, H.; Toyota, T. & Uto, S. (2002). Sea ice thickness estimated from passive microwave radiometers, *Polar Meteorology and Glaciology*, Vol. 16, pp.15-31.
- Thorndike, A.S.; Rothrock, D.A.; Maykut, G.A. & Colony, R. (1975). The thickness distribution of sea ice, *J. Geophys. Res.*, Vol. 80, No. 33, pp. 4501-4513.
- Toyota, T.; Kawamura, T.; Ohshima, K.I.; Shimoda, H. & Wakatsuchi, M. (2004). Thickness distribution, texture and stratigraphy, and a simple probabilistic model for dynamical thickening of sea ice in the southern Sea of Okhotsk, *J. Geophys. Res.*, Vol.109, C06001, doi:10.1029/2003JC002090.
- Toyota, T.; Takatsuji, S.; Tateyama, K.; Naoki, K. & Ohshima, K.I. (2007). Properties of sea ice and overlying snow in the southern Sea of Okhotsk, *J. Oceanogr.*, Vol.63, No.3, pp. 393-411.
- Toyota, T.; Nakamura, K.; Uto, S.; Ohshima, K.I. & Ebuchi, N. (2009). Retrieval of sea ice thickness distribution in the seasonal ice zone from airborne L-band SAR, *Int. J. Remote Sens.*, Vol. 30, No. 12, pp. 3171-3189.
- Troy, B.E.; Hollinger, J.P.; Lerner, R.M. & Wisler, M.M. (1981). Measurement of the microwave properties of sea ice at 90 GHz and lower frequencies, *J. Geophys. Res.*, Vol. 86, No.C5, pp. 4283-4289.
- Tucker, W.B. ; Weatherly, J.W. ; Eppler, D.T. ; Farmer, L.D. & Bentley, D.L. (2001). Evidence for rapid thinning of sea ice in the weatern Arctic Ocean at the end of the 1980s, *Geophys. Res. Lett.*, Vol.28, No.14, pp. 2851-2854.
- Uto, S.; Shimoda, H. & Ushio, S. (2006a). Characteristics of sea-ice thickness and snow-depth distributions of the summer landfast ice in Lützow-Holm Bay, East Antarctica, *Ann. Glaciol.*, Vol.44, pp. 281-287.
- Uto, S.; Toyota, T.; Shimoda, H.; Tateyama, K. & Shirasawa, K. (2006b). Ship-borne electromagnetic induction sounding of sea-ice thickness in the southern Sea of Okhotsk, *Ann. Glaciol.*, Vol. 44, pp. 253-260.
- Vant, M.R.; Ramseier, R.O. & Makios, V. (1978). The complex-dielectric constant of sea ice at frequencies in the range 0.1-40 GHz, *J. Appl. Phys.*, Vol. 49, No.3, pp.1264-1280.

- Vinje, T.; Nordlund, N. & Kvambekk, A. (1998). Monitoring ice thickness in Fram Strait, *J. Geophys. Res.*, Vol.103, No.C5, pp.10437-10449.
- Wadhams, P. & Horne, R.J. (1980). An analysis of ice profiles obtained by submarine sonar in the Meaufort Sea, *J. Glaciol.*, Vol.25, No.93, pp. 401-424.
- Wadhams, P. (1983). Sea ice thickness distribution in Fram Strait, *Nature*, Vol.305, pp. 108-111.
- Wadhams, P.; McLaren, A.S. & Weintraub, R. (1985). Ice thickness distribution in Davis Strait in February from submarine sonar, *J. Geophys. Res.*, Vol.90, No.C1, pp. 1069-1077.
- Wadhams, p. (1988). The underside of Arctic sea ice imaged by sidescan sonar, *Nature*, Vol.333, pp.161-164.
- Wadhams, P. (1990). Evidence for thinning of the Arctic ice cover north of Greenland, *Nature*, Vol.345, pp. 795-797.
- Wadhams, P. (1992). Sea ice thickness distribution in the Greenland Sea and Eurasian Basin, May 1987, *J. Geophys. Res.*, Vol.97, No.C4, pp. 5331-5348.
- Wadhams, P. (2000). *Ice in the Ocean*, Gordon and Breach Science Publishers, ISBN 90-5699-296-1, Amsterdam, The Netherlands.
- Wakabayashi, H.; Matsuoka, T.; Nakamura, K. & Nishio, F. (2004). Polarimetric characteristics of sea ice in the Sea of Okhotsk observed by airborne L-band SAR, *IEEE Trans. Geosci. Remote Sensing*, Vol. 42, No. 11, 2412-2425.
- Wilheit, T.; Nordberg, W.; Blinn, J.; Campbell, W. & Edgerton, A. (1972). Aircraft measurements of microwave emission from Arctic sea ice, *Remote Sensing of Environment*, Vol. 2, pp.129-139.
- Winebrenner, D.P.; Tsang, L.; Wen, B & West, R. (1989). Sea ice characterization measurements needed for testing of microwave remote sensing models, *IEEE J. Oceanic Eng.*, Vol. 14, No.2, pp. 149-158.
- Worby, A.P.; Jeffries, M.O.; Weeks, W.F.; Morris, K. & Jana, R. (1996). The thickness distribution of sea ice and snow cover during late winter in the Bellingshausen and Amundsen Seas, Antarctica, *J. Geophys. Res.*, Vol.101, pp. 28441-28455.
- Worby, A.P.; Griffin, P.W.; Lytle, V.I. & Massom, R.A. (1999). On the use of electromagnetic induction sounding to determine winter and spring sea ice thickness in the Antarctic, *Cold Reg. Sci. Technol.*, Vol. 29, pp.49-58.
- Worby, A.P. & Allison, I. (1999). A technique for making ship-based observations of Antarctic sea ice thickness and characteristics, *ANTARCTIC CRC Research Report*, No.14, pp. 1-63.
- Worby, A.P.; Bush, G.M. & Allison, I. (2001). Seasonal development of the sea-ice thickness distribution in East Antarctica: measurements from upward-looking sonars, *Ann. Glaciol.*, Vol.33, pp.177-180.
- Worby, A.P.; Geiger, C.A.; Paget, M.J.; Van Woert, M.L.; Ackley, S.F. & DeLiberty, T.L. (2008). Thickness distribution of Antarctic sea ice, *J. Geophys. Res.*, Vol.113, C05S92, doi:10.1029/2007JC004254.
- Zubov, N.N. (1945). Arctic ice, Izdatel'stvo Glavsermorputi, Moscow, 360pp. (Translated to Japanese by Institute of Low Temperature Science, Hokkaido Univ. in 1958).
- Zwally, H.J.; Yi, D.; Kwok, R. & Zhao, Y. (2008). ICESat measurements of sea ice freeboard and estimates of sea ice thickness in the Weddell Sea, *J. Geophys. Res.*, Vol. 113, C02S15, doi:10.1029/2007JC004284.



## **Advances in Geoscience and Remote Sensing**

Edited by Gary Jedlovec

ISBN 978-953-307-005-6

Hard cover, 742 pages

**Publisher** InTech

**Published online** 01, October, 2009

**Published in print edition** October, 2009

Remote sensing is the acquisition of information of an object or phenomenon, by the use of either recording or real-time sensing device(s), that is not in physical or intimate contact with the object (such as by way of aircraft, spacecraft, satellite, buoy, or ship). In practice, remote sensing is the stand-off collection through the use of a variety of devices for gathering information on a given object or area. Human existence is dependent on our ability to understand, utilize, manage and maintain the environment we live in - Geoscience is the science that seeks to achieve these goals. This book is a collection of contributions from world-class scientists, engineers and educators engaged in the fields of geoscience and remote sensing.

### **How to reference**

In order to correctly reference this scholarly work, feel free to copy and paste the following:

Takenobu Toyota (2009). Application of Remote Sensing to the Estimation of Sea Ice Thickness Distribution, *Advances in Geoscience and Remote Sensing*, Gary Jedlovec (Ed.), ISBN: 978-953-307-005-6, InTech, Available from: <http://www.intechopen.com/books/advances-in-geoscience-and-remote-sensing/application-of-remote-sensing-to-the-estimation-of-sea-ice-thickness-distribution>

**INTECH**  
open science | open minds

### **InTech Europe**

University Campus STeP Ri  
Slavka Krautzeka 83/A  
51000 Rijeka, Croatia  
Phone: +385 (51) 770 447  
Fax: +385 (51) 686 166  
[www.intechopen.com](http://www.intechopen.com)

### **InTech China**

Unit 405, Office Block, Hotel Equatorial Shanghai  
No.65, Yan An Road (West), Shanghai, 200040, China  
中国上海市延安西路65号上海国际贵都大饭店办公楼405单元  
Phone: +86-21-62489820  
Fax: +86-21-62489821

© 2009 The Author(s). Licensee IntechOpen. This chapter is distributed under the terms of the [Creative Commons Attribution-NonCommercial-ShareAlike-3.0 License](https://creativecommons.org/licenses/by-nc-sa/3.0/), which permits use, distribution and reproduction for non-commercial purposes, provided the original is properly cited and derivative works building on this content are distributed under the same license.

IntechOpen

IntechOpen